iScience

CellPress
OPEN ACCESS

Article

Energy transfer and trapping in photosystem I with and without chlorophyll-*f*

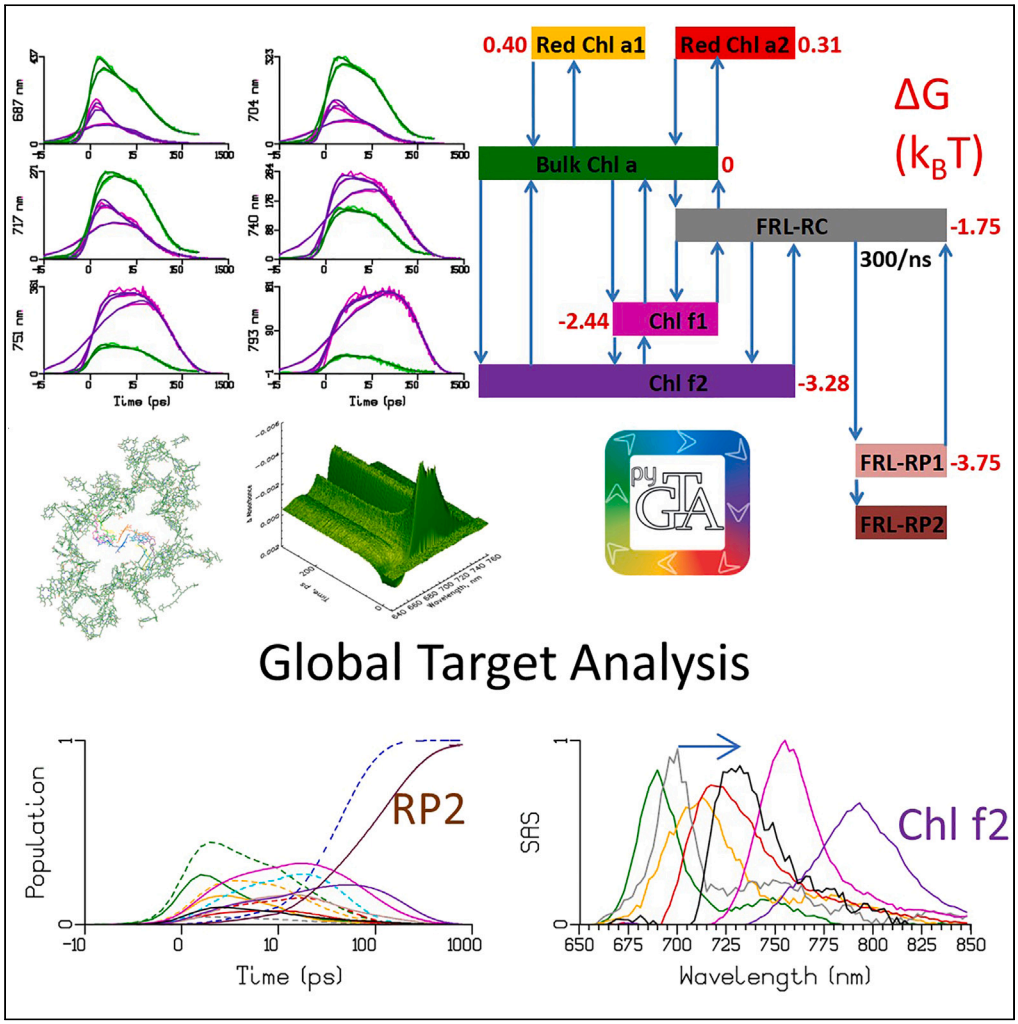

Ivo H.M. van Stokkum, Marc G. Müller, Jörn Weißenborn, Sebastian Weigand, Joris J. Snellenburg, Alfred R. Holzwarth

i.h.m.van.stokkum@vu.nl

Highlights

Properties of white light and far-red light grown photosystem I reaction centers differ

The lowest excited state of the FRL-RC is lowered by ≈29 nm, and is ≈k_BT above Chl *f*

The rate of charge separation drops from ≈900 ns^{-1} in WL-RC to ≈300 ns^{-1} in FRL-RC

Trapping in FRL-PSI occurs after uphill energy transfer from the Chl *f* compartments

van Stokkum et al., iScience *26*, 107650
September 15, 2023
https://doi.org/10.1016/j.isci.2023.107650

iScience

CellPress
OPEN ACCESS

Article

Energy transfer and trapping in photosystem I with and without chlorophyll-*f*

Ivo H.M. van Stokkum,[1,3,*] Marc G. Müller,[2] Jörn Weißenborn,[1] Sebastian Weigand,[1] Joris J. Snellenburg,[1] and Alfred R. Holzwarth[1,2]

SUMMARY

We establish a general kinetic scheme for energy transfer and trapping in the photosystem I (PSI) of cyanobacteria grown under white light (WL) or far-red light (FRL) conditions. With the help of simultaneous target analysis of all emission and transient absorption datasets measured in five cyanobacterial strains, we resolved the spectral and kinetic properties of the different species present in PSI. WL-PSI can be described by Bulk Chl *a*, two Red Chl *a*, and a reaction center compartment (WL-RC). The FRL-PSI contains two additional Chl *f* compartments. The lowest excited state of the FRL-RC is downshifted by ≈ 29 nm. The rate of charge separation drops from ≈900 ns^{-1} in WL-RC to ≈300 ns^{-1} in FRL-RC. The delayed trapping in the FRL-PSI (≈130 ps) is explained by uphill energy transfer from the Chl *f* compartments with Gibbs free energies of ≈k_BT below that of the FRL-RC.

INTRODUCTION

Photosynthesis is key to the conversion of solar energy to biomass.[1] Light harvesting antennae absorb sunlight and transfer the excitation energy ultimately to the reaction centers (RCs). The charge separation in the RC of Photosystem I (PSI)[2–5] is part of an electron transport chain, the *Z*-scheme of oxygenic photosynthesis.[6] A typical PSI complex of cyanobacteria consists of eight proteins that bind more than 90 chlorophyll *a* (Chl *a*) pigments and 22 β-carotenes.[2] In all cyanobacterial PSI complexes "Red Chl *a*" pigments are present that enhance the absorption cross section above 700 nm.[7–17] An excitation of a lower energy "Red Chl *a*" pigment is transferred uphill to the RC, where ultrafast charge separation can occur.[18] More recently, PSI complexes containing Chl *d* or Chl *f*[19–22] in their antenna have been demonstrated to photochemically trap even more red light.[23–30] Thus, PSI of cyanobacteria grown under far-red light (FRL) conditions can absorb and utilize FRL of wavelengths up to 800 nm by integrating the redshifted Chl *f* in the antenna, whereas PSI of cyanobacteria grown under white light (WL) conditions can absorb and utilize red light of wavelengths up to 730 nm via their "Red Chl *a*" pigments. Here we will develop a general kinetic scheme for energy transfer and trapping that explains how all the light energy can be utilized in PSI complexes with and without Chl *f* (see Video S1).

On the lumenal side of the PSI complex is the RC, which contains six excitonically coupled Chl *a* pigments.[18,31–34] The electron transport chain has two branches (A and B) composed of several cofactors: (i) a Chl *a*′/Chl *a* pair (ec1A/ec1B) traditionally called P700, (ii) in each branch is a pair of Chl *a* molecules (ec2A/ec3A or ec2B/ec3B)[34] and a phylloquinone (PhQA or PhQB), and (iii) the branches join again at the F_X iron-sulfur (FeS) cluster and two more FeS (A and B) finalize the delivery of the electron on the stromal side of the membrane, where it is transferred to ferredoxin. In contrast to PSII, the PSI RC cannot be separated from its antenna, and therefore the PSI complex must be studied in its entirety. In time-resolved spectroscopy experiments the spectral evolution of a PSI complex that has absorbed a photon is monitored. High time-resolution fluorescence experiments, simultaneously registering the time-resolved spectrum with the help of a streak camera,[35] provide excellent information on excitation energy transfer (EET)[36] between the different excited states, and the disappearance of the emission indicates the trapping by charge separation.[12–14,30,37] To study the mechanism of the charge separation and the radical pair dynamics experimentally challenging low-power transient absorption experiments are mandatory.[38–40] In both types of experiments care needs to be taken to avoid annihilation due to the absorption of more than one photon by the PSI complex.[30,38,40,41] Time-resolved fluorescence low-power experiments are relatively easier and allow concentrating on the dynamics of EET and trapping that occur concomitantly. To understand a system with ≈100 different pigments is challenging. Since the EET between neighboring Bulk Chl *a* pigments takes <100 fs[33], all Bulk Chl *a* pigments (which possess identical spectra) can be lumped into a single Bulk Chl *a* compartment. Analogously, "Red Chl *a*" or Chl *f* pigments that possess identical spectra can be lumped into "Red Chl *a*" or Chl *f* compartments. The RC will be considered a single compartment, which consists of the six excitonically coupled Chl *a* pigments. Global and target analysis of all experiments employs a functional compartmental model[42] with microscopic rate constants that connect the different compartments to estimate the parameters that describe the dynamics of

[1]Department of Physics and Astronomy and LaserLaB, Faculty of Science, Vrije Universiteit Amsterdam, De Boelelaan 1081, Amsterdam 1081 HV, the Netherlands
[2]Max-Planck-Institut für chemische Energiekonversion, 45470 Mülheim a.d. Ruhr, Germany
[3]Lead contact
*Correspondence: i.h.m.van.stokkum@vu.nl
https://doi.org/10.1016/j.isci.2023.107650

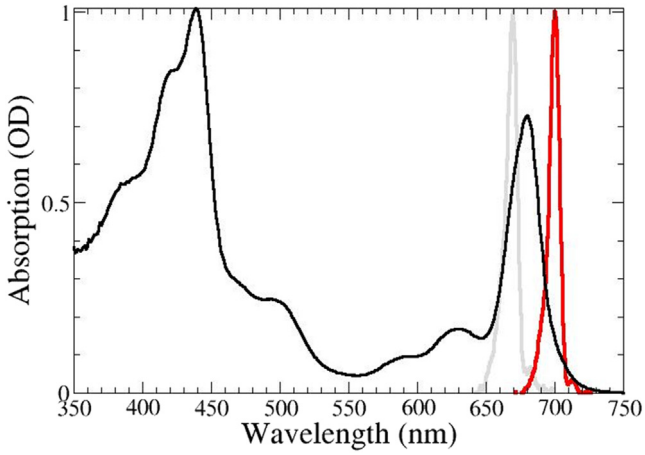

Figure 1. Absorption spectrum (black) of the WL-PSI complexes from SCy6803
Spectra of the excitatory pulse, key: 670 (gray) and 700 nm (red).

the PSI complex.[15,42,43] The kinetic schemes for PSI that have been proposed so far focus on the equilibration between Bulk Chl *a* and "Red Chl *a*" in the antenna by analyzing the fluorescence[13] or focus on the charge separation by analyzing the transient absorption.[40,44,45]

In this paper we investigate the mechanism of trapping in the FRL-RC, and how this enables the harvesting of the FRL. To this end we develop a general kinetic scheme for EET and trapping in the PSI of five cyanobacterial strains grown under WL or FRL conditions.[30] First, to establish the ultrafast dynamics in WL-PSI, the PSI transient absorption of WL-grown Synechocystis PCC6803 (SCy6803) is studied here in the reduced form. Second, time-resolved fluorescence is studied in WL-PSI and FRL-PSI of four cyanobacterial strains possessing different Chl *f* absorption profiles. Third, the transient absorption of both WL- and FRL-grown Fischerella thermalis strain PCC 7521 (FT7521)[27] completes the data needed to identify the mechanism of trapping in the FRL-RC. In transient absorption different excitation wavelengths have been used to selectively excite the different pigment pools, thus enhancing their resolvability. The charge separation will be described by a simplified scheme with two radical pairs, RP1 and RP2. We will demonstrate that all time-resolved experiments in cyanobacteria that contain highly diverse antenna pigments can be described by a common functional compartmental model,[42] with different RC properties of the WL-PSI and FRL-PSI. Only by combining all the information from the different experiments can the properties of the many different species (Bulk Chl *a*, two Red Chl *a* pools, WL-RC, WL-RP1, WL-RP2, two Chl *f* pools, FRL-RC, FRL-RP1, and FRL-RP2) be resolved. The determined kinetic schemes describe the dynamics of energy transfer and charge separation and the radical pair yield of WL-PSI and FRL-PSI complexes under all excitation conditions. We will demonstrate how the properties of the RC differ in WL and FRL grown PSI.

RESULTS AND DISCUSSION

Data with global analysis of transient absorption in SCy6803

In ultrafast transient absorption experiments on WL-PSI complexes of SCy6803 in the reduced form two excitation wavelengths have been used (Figure 1): 670 nm which selectively excites Chl *a* pigments absorbing to the blue of the Bulk Chl *a*,[42,46–48] and 700 nm which excites the RC, the "Red Chl *a*" pigments and the Bulk Chl *a* antenna. Representative traces and fits are depicted in Figure 2. The quality of the global analysis fit is excellent (Figures S1–S3). A small amount of free Chl *a* is responsible for the slight difference in the final level at 685 nm (Figure 2A). The difference between the colored traces representing the two excitation wavelengths is very informative. The kinetics with 670 (black) and 700 (red) nm excitations differ until ≈10 ps. A small amount of relatively slow equilibration is clearly visible near 700 nm (Figure 2B, where the black and red lines cross near 3 ps). A "coherent artifact" (CA) straddling time zero is present in the transient absorption of Figure 2. The analysis thereof is presented in Figure S4. Here we present the global analysis results of each experiment using a sequential kinetic scheme consisting of five components with increasing lifetimes. The Evolution Associated Difference Spectra (EADS) estimated with 670 and 700 nm excitation are depicted in Figures 3A and 3B, respectively, whereas the accompanying Decay Associated Difference Spectra (DADS) are shown in Figures 3E and 3F. The EADS focus on the spectral evolution, whereas the DADS highlight the decay or rise of spectral bands with the estimated lifetimes. With 670 nm excitation the gray to orange evolution (0.36 ps) can be attributed to ultrafast equilibration of the initially excited antenna states with the Bulk Chl *a* states, as evidenced by a shift to lower energy of the bleach plus stimulated emission (BL + SE) (Figure 3A), and by the decay around ≈675 nm and the rise around ≈690 nm (gray DADS in Figure 3E). The orange to cyan evolution (2.6 ps) can be attributed to equilibration between the Bulk Chl *a* and the Red Chl *a* states, as evidenced by the decay of BL + SE around ≈685 nm and the rise of BL + SE around ≈710 nm (orange DADS in Figure 3E). The green EADS (evolving in 16 ps) is dominated by features of the first radical pair, i.e., a bleaching with a minimum at 685 nm, which agrees with the literature,[27,40,49] whereas the magenta EADS (evolving in 26 ps) can be attributed to the second radical pair. With 700 nm excitation (Figure 3B) the first lifetime has been fixed at 0.1 ps (black EADS) and is a mixture of the initially excited state (attributable to the excited Red Chl *a* and WL-RC) and the CA. Overlapping in time with the CA is the equilibration within the directly excited RC in ≈100 fs. Thus, the 0.1 ps DADS (black in Figure 3F) and the IRFAS

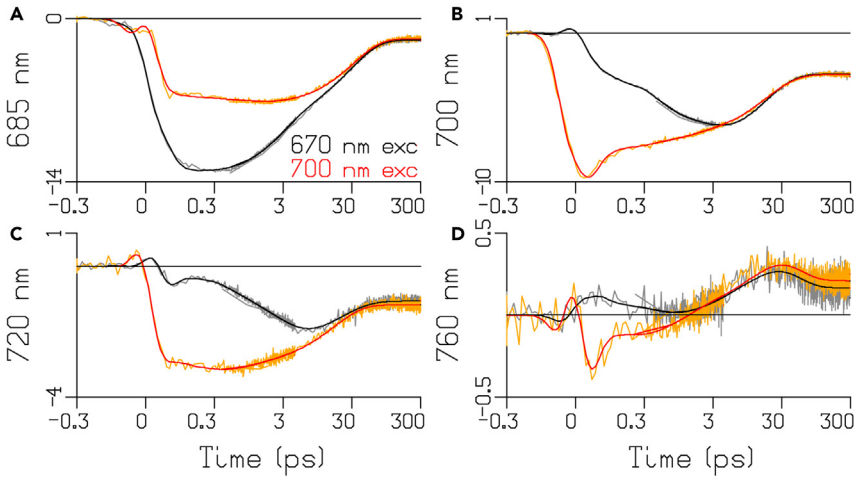

Figure 2. Transient absorption data and fit of WL-PSI complexes of SCy6803

(A–D) Transient absorption (in units of mOD) of SCy6803 WL-PSI at four selected wavelengths (indicated in the ordinate label). Key: 670 nm excitation (gray), 700 nm excitation (orange). Black and red lines indicate the global analysis fit. Note that the time axis is linear until 0.3 ps and logarithmic thereafter. Note also that each panel is scaled to its maximum. The overall rms error of the fit was 0.067 mOD.

(Figure S4C) also contain contributions from the rise of the BL + SE around 680 nm. A more detailed analysis of this is beyond the scope of this paper. It has been claimed[44] that after 760 nm excitation spectral features of RP1 are present before 180 fs. Here we found no evidence of ultrafast charge separation, and we attribute the ultrafast dynamics to CA and equilibration between the excitonically connected pigments within the directly excited RC. The 1 ps DADS (red in Figure 3F) show a decay of BL + SE around ≈700 nm and a rise of BL + SE around ≈680 nm. In 1 ps the red EADS evolves to the blue EADS, a subtle evolution that again can only be interpreted with the help of a target analysis. Note also that there are subtle differences between the cyan and blue EADS (cf. the overlay in Figure 3C), which indicate equilibration on a timescale longer than 2.6 ps. Analogous to Figure 3A (cf. the overlay in Figure 3D), the dark green EADS (evolving in 17 ps) is dominated by features of the first radical pair (the bleaching with a minimum at 685 nm), whereas the purple EADS (evolving in 26 ps) can be attributed to the second radical pair. The small difference around 675 nm in Figure 3D can be assigned to a small amount of free Chl *a*. These ten EADS and DADS can only be interpreted with the help of a target analysis using the kinetic scheme of Figure 4A.

Target analysis of transient absorption of WL-PSI in SCy6803

To characterize the trapping, the data are simultaneously analyzed with a simplified kinetic scheme with trapping from a WL-RC compartment, which consists of the six excitonically coupled Chl *a* pigments. In the kinetic scheme of the reduced form (Figure 4A) the mechanism of the charge separation is highly simplified, neglecting the equilibration within the RC and disregarding the charge separation in two separate branches A and B.[40,49,50] It is further assumed that the charge separation can be approximated by a two-step process. We found that the data could not be fitted satisfactorily by a kinetic scheme with fewer compartments. To perform a simultaneous target analysis with a minimal number of Species Associated Difference Spectra (SADS), all SADS have been linked between the two experiments (Figure 4). The quality of the target analysis fit is excellent (Figure S5).

First, we discuss the populations of Figure 4B. The amplitude matrices after 670 and 700 nm excitations are given in Tables S1A and S1B, respectively. After 670 nm excitation ultrafast equilibration takes place in 0.37 ps (light and dark green solid lines). Subsequently, the RC population rises, mainly with 0.54 ps (black solid line). With lifetimes of 1.78 and 6.36 ps further equilibration between the Bulk Chl *a* and the Red Chl *a1* and *a2* takes place, and the RP1 population rises (cyan solid line). The RP2 population rises with ≈15 ps (blue solid line), and the excitations are trapped from the equilibrated RC with ≈23 ps. The main differences with 700 nm excitation are the virtual absence of the 0.37 ps equilibration and the immediate rise of RP1 with 0.54 ps (cyan dashed line), since 20% of the excitations directly excites the RC (black dashed line). In addition, the directly excited Red Chl *a1* and *a2* populations persist (orange and red dashed line) until they decay via trapping from the equilibrated RC with ≈23 ps. The RP1 decays to RP2 in ≈15 ps, in agreement with the global analysis result of Figure 3, where we estimated lifetimes of ≈16 and 26 ps for the two final evolutions. Finally, the excitations in the fully equilibrated PSI are trapped in ≈23 ps. The quantum yield in PSI is 99.0% (Table S1, long lived column).

Next, we discuss the estimated SADS. The Bulk Chla SADS (dark green in Figure 4C) exhibits a broad BL + SE band with a minimum at 686 nm, and a small excited state absorption (ESA) below 665 nm. With 670 nm excitation an initially excited antenna compartment Ant1 (light green) is needed, with an SADS shifted to higher energy relative to the Bulk Chl *a* SADS (light vs. dark green in Figure 4C). SCy6803 contains two Red Chl *a* pools (orange and red in Figure 4). The estimated SADS of these Red Chl *a* species exhibit broad BL + SE bands with minima near 703 and 712 nm, and ESA with maxima around 670 nm (orange and red in Figure 4C). The WL-RC SADS (black in Figures 4C and 4D) exhibits a broad BL + SE band with a minimum around 692 nm, and ESA below 680 nm. Note that both Red Chl *a* SADS are red shifted relative

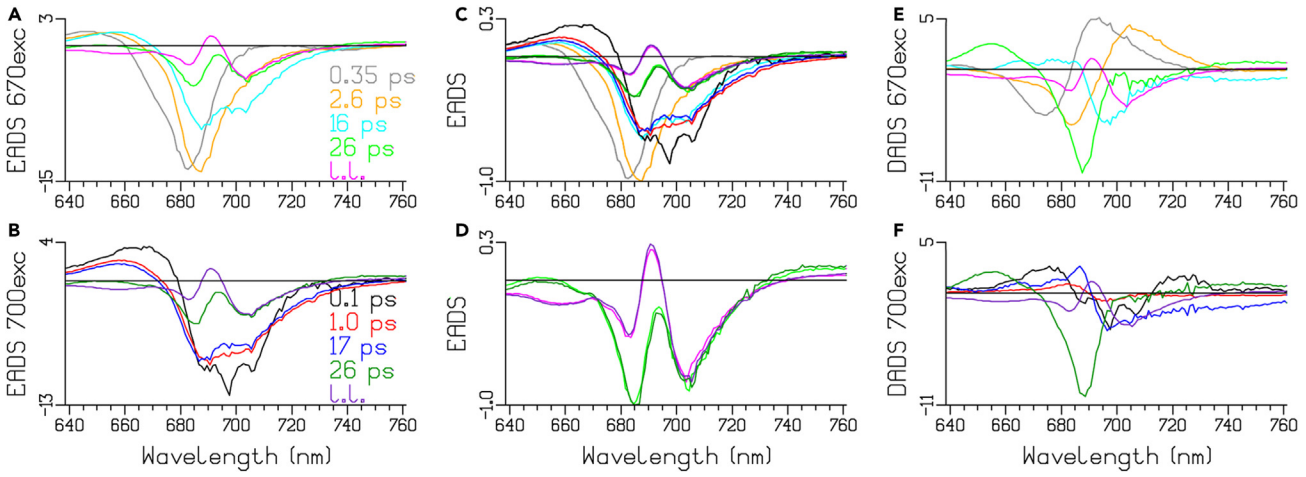

Figure 3. Global analysis of transient absorption from WL-PSI complexes of SCy6803

Evolution Associated Difference Spectra (EADS, mOD) in PSI complexes of SCy6803 estimated with 670 (A) and 700 (B) nm excitation, and overlays (C and D, scaled to the minimum). Decay Associated Difference Spectra (DADS, mOD) (E and F). Key 670 exc: gray, 0.36 ps; orange, 2.6 ps; cyan, 16 ps; green, 26 ps; magenta, long lived. Key 700 exc: black, 0.1 ps; red, 1.0 ps; blue, 17 ps; dark green, 26 ps; purple, long lived.

to the WL-RC SADS. The RP2 SADS demonstrates the bleach of the cation (P^+700) and a large electrochromic shift at 688 nm (blue in Figure 4D). The phylloquinone anion of RP2 does not absorb in this wavelength region. The SADS of RP1 has a bleaching with a minimum at 685 nm, which agrees with the literature.[27,40,49] The difference between the RP1 and RP2 SADS can be attributed to the Chl *a* anion of RP1, absorbing below 660 and above 694 nm (compare the cyan and blue SADS in Figure 4D). The size of this difference is smaller than the SADS of the Bulk Chl *a*, since the latter also contains the stimulated emission.

The location of the extremum of the bleach plus stimulated emission (in wavenumber, $\overline{\nu}_{max}$, or in wavelength, λ_{max}) of the SADS can be estimated with the help of skewed Gaussian shapes.[43] This is employed to compute the enthalpy difference ΔH relative to Bulk Chl *a* in units of k_BT (row 4 in Table 1). Using the Gibbs free energy difference (relative to Bulk Chl *a*) ΔG computed from the kinetic scheme in Figure 4A, the entropy difference (relative to Bulk Chl *a*) is computed from ΔH-$\Delta G = T\Delta S$. Finally, the number of pigments in the compartments "N" is estimated from the entropy difference ($N = N_{Bulk} \exp(\Delta S/k_B)$) and shown in the bottom row of Table 1. This results in estimates of almost two pigments for the Ant1 and Red Chl *a2* compartments, and of 4.8 pigments for the Red Chl *a1* compartment. The estimate for the WL-RC compartment is larger than the expected six pigments. Precise quantification of the number of pigments in each compartment is difficult, since it crucially depends on the validity of the many assumptions that have been used in the target analysis. Also, in view of the excitonic interactions involved in many of the compartments, the numbers in the bottom row of Table 1 should be interpreted cautiously.

The kinetic scheme used for the target analysis of the TA experiments of SCy6803 (Figure 4A) can well describe the sub-ps kinetics (Figure S5), thus establishing the rate of trapping. Note that the Gibbs free energy of the Bulk Chl *a* is the lowest of all excited state compartments implying that uphill EET to the WL-RC precedes the ultrafast charge separation. We estimate that the charge recombination rate from WL-RP1 to WL-RC is very small (5 ns^{-1}), resulting in a Gibbs free energy difference of more than 5 k_BT. Thus, the primary charge separation in the WL-RC is virtually irreversible. In all the kinetic schemes of the WL grown PSI complex used in this paper we fix the rate of trapping at 900 ns^{-1} and the Gibbs free energy difference between WL-RC and Bulk Chl *a* at 1.50 k_BT. This rate of trapping agrees with the estimate of $\approx$1 ps^{-1} based upon a lattice model.[18] It also agrees with the recently estimated value of $\approx$750 ns^{-1} at 77 K.[51]

Target analysis of WL-PSI and FRL-PSI of SCo7335, CF9212, FT7521, and CT7203

The kinetic schemes of Figure 5 describe the emission experiments of WL and FRL grown SCo7335, CF9212, FT7521, and CT7203. The parameters have been estimated from a simultaneous target analysis also including the transient absorption experiments of WL and FRL grown FT7521 (Figure 7). We will first discuss the emission results, the populations and the estimated Species Associated Spectra (SAS) of the four strains (Figure 6), before turning to the transient absorption results of FT7521.

The kinetic schemes used for the target analyses of the experiments of WL grown SCo7335 (Figure 5A) and for the TA experiments of SCy6803 (Figure 4A) are generally consistent, although the estimated rate constants are somewhat different. Importantly, both target analyses are consistent with a rate of primary charge separation of 900 ns^{-1}.

A simultaneous target analysis of the WL-PSI and FRL-PSI experiments of each cyanobacterial strain has been performed, thus ensuring consistency, and requiring a minimum number of free parameters. The parameters of the CF9212, FT7521, and CT7203 strains have been linked as much as possible since the strains behave similarly. The connectivity in the kinetic scheme (Figure 5) of the target analysis of WL-PSI is the same as in Figure 4A. Analogously to SCy6803, two different Red Chl *a* compartments are needed. The quality of the target analysis fit is very good (Figures S7–S10). The free energies of the Red Chl *a1* and *a2* compartments relative to the Bulk Chl *a* range from 0.08 to 1.28 k_BT (Figure 5). This is attributed to slightly different properties or amounts of the Red Chl *a1* and *a2* pigments in the

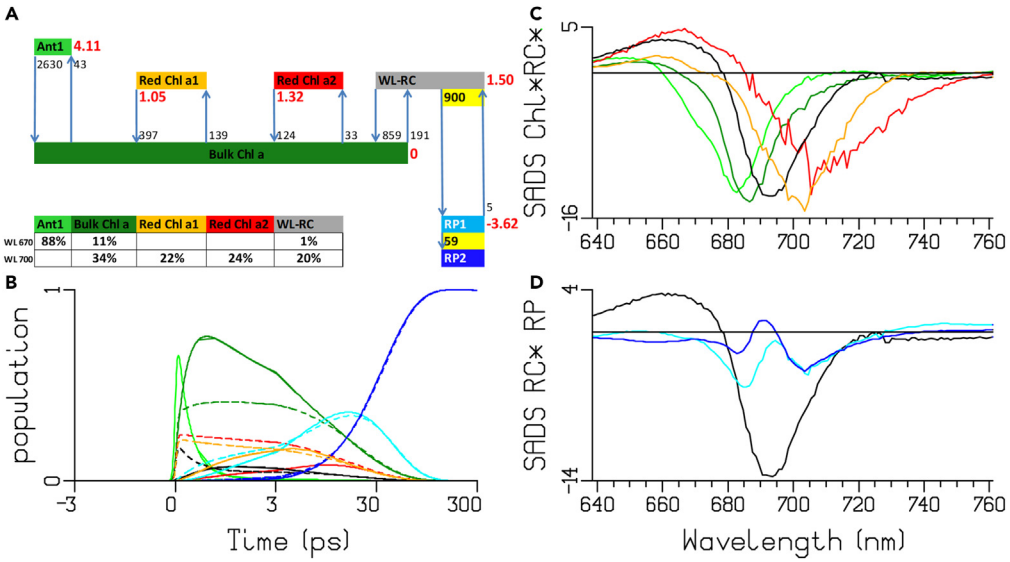

Figure 4. Target analysis of transient absorption from WL-PSI complexes of SCy6803

Kinetic scheme with rates in ns^{-1}. Each compartment is represented by a colored box. The initial populations are indicated in panel (A), below left. Red numbers indicate the free energy relative to Bulk Chl *a* (in k_BT = 25.2 meV, 20°C). The trapping rates are highlighted yellow. For clarity, the natural decay rates of the excited states and the free Chl *a* have been omitted. Populations (B) and SADS (C and D, in mOD). Line type key: 670 nm excitation (solid), 700 nm excitation (dashed). Color key: Ant1 (light green), Bulk Chl *a* (dark green), Red Chl *a1* (orange) and *a2* (red), WL-RC (black), RP1 (cyan), and RP2 (blue). Note that the time axis in (B) is linear until 3 ps and logarithmic thereafter.

four strains (cf. the different relative amplitudes of the orange and red curves in Figures 6A, 6C, 6E, and 6G). In contrast to WL-PSI, FRL-PSI contains two Chl *f* compartments (cf. Figure 5, right hand side) that harvest the FRL and emit at wavelengths longer than 740 nm. Their free energy is much lower than that of Bulk Chl *a*, by 1.98–3.28 k_BT (Figure 5). Some of the Chl *f* pigments (magenta and purple in Figures 5 and 6) are located in the vicinity of the RC but not in the RC,[22] in agreement with the observed quenching of their emission by the oxidized RC at 77K.[30] The free energy of the RC relative to the Bulk Chl *a* is 1.5 k_BT for WL-PSI, and ≈−1.75 k_BT for FRL-PSI. In[30] it has been proposed that in the FRL-PSI the RC is altered, so as to allow for charge separation after uphill EET from Chl *f1* at 77K. Assuming that the FRL-RC at 77K is similar to that at RT, uphill EET from Chl *f1* would be possible, thus confirming the proposal of.[30] Compared to the target analysis of,[30] which was limited to the decay associated spectra of Chl *f1* and Chl *f2*, this uphill EET from Chl *f1* is the main point of agreement. Another common finding is that the trapping of Chl *f2* excitations is faster than the trapping of Chl *f1* excitations; here we estimated rates of 8 and 6 ns^{-1} to FRL-RC from Chl *f* (Figure 5). This indicates that the Chl *f2* pigments are located somewhat closer to the FRL-RC. The kinetic scheme of Tros et al.[30] aims to describe only the two Chl *f* compartments, whereas in the schemes of Figure 5 *all* data are described with seven emissive species. At 77 K, evidence was found of downhill EET from the Red Chl *a* and the high energy Chl *f* containing compartments ultimately to the lowest energy Chl *f* containing compartment.[30] At RT, the estimated downhill rates from Chl *f1* to Chl *f2* range from ≈2.7–7.6 ns^{-1} (Figure 5). The largest downhill rate (7.6 ns^{-1}) is found with FT7521, where the selective 740 nm excitation transient absorption experiment dominantly populates both Chl *f* compartments (Figure 7F, 68% and 27%, cf. the dashed lines in Figure 7G discussed in the following) thus providing the information on their equilibration.

Table 1. Thermodynamic properties of the Scy6803 species

	Ant1	Bulk Chl *a*	Red Chl *a1*	Red Chl *a2*	WL-RC
λ_{max} (nm)	684	689	705	715	695
$\overline{V}_{max}$ (cm^{-1})	14612	14509	14194	13979	14387
$\overline{V}_{max}$ (k_BT)	75.3	74.8	73.2	72.1	74.2
ΔH (k_BT)	0.5		−1.6	−2.7	−0.6
ΔG (k_BT)	4.1		0.7	0.1	1.4
ΔH-ΔG = TΔS (k_BT)	−3.6		−2.3	−2.8	−2.0
"N"	2.2	78	7.7	4.7	10.5

Location of the extremum of the bleach plus stimulated emission estimated from the SADS in Figure 4C: λ_{max} in nm, $\overline{V}_{max}$ in cm^{-1} and in k_BT (1 k_BT = 207 cm^{-1}). ΔH relative to Bulk Chl *a* in k_BT. ΔG taken from Figure 4A. ΔH-ΔG = TΔS (k_B.T) and "N" is computed via $N = N_{Bulk} \exp(\Delta S/k_B)$.

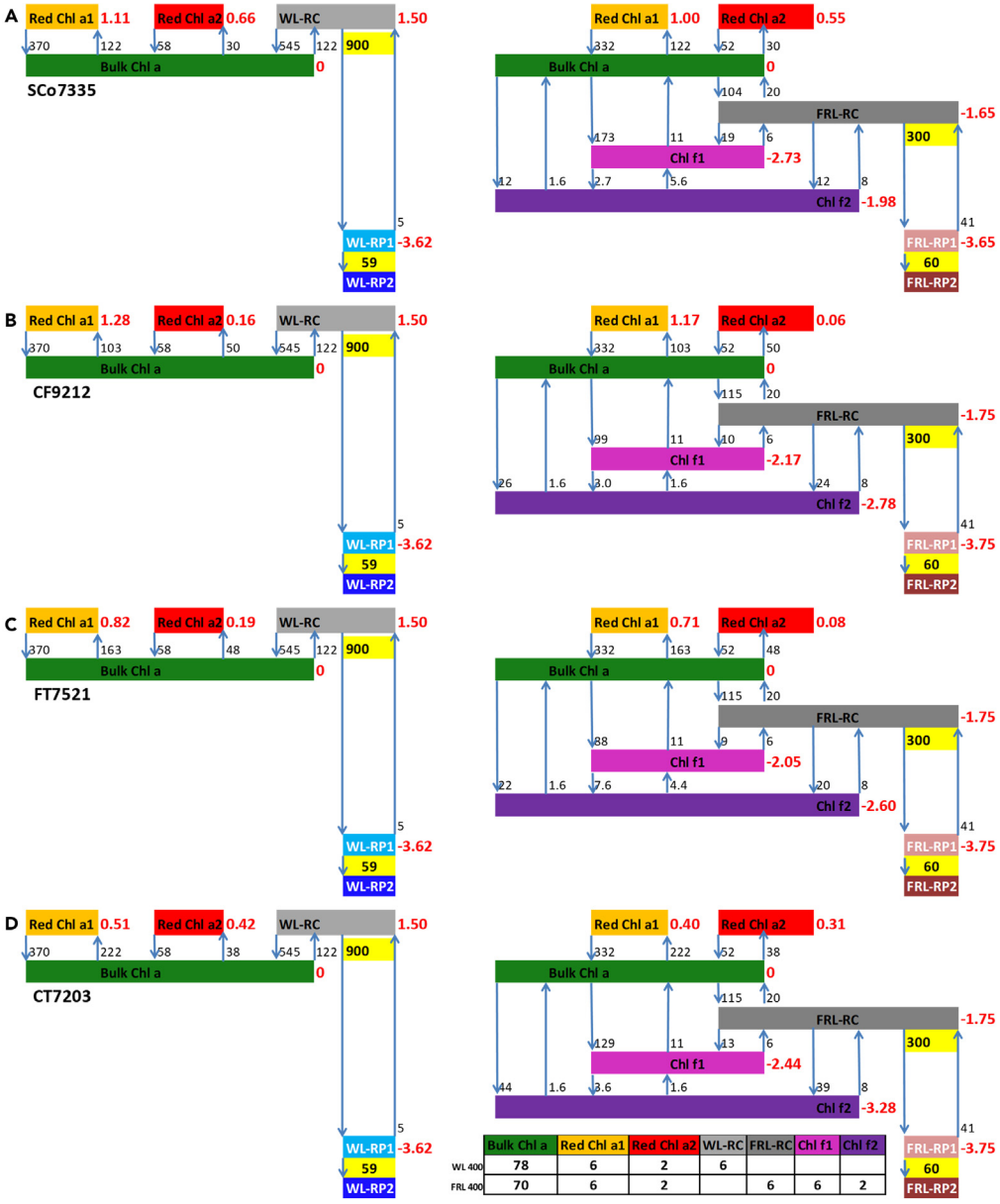

Figure 5. Kinetic schemes with rates in ns^{-1} of WL-PSI (left) and FRL-PSI (right) complexes of SCo7335, CF9212, FT7521, and CT7203 at RT

(A–D) Each compartment is represented by a colored box. Key: Bulk Chl *a* (dark green), Red Chl *a1* (orange), Red Chl *a2* (red), WL-RC (gray), FRL-RC (black), Chl *f1* (magenta), Chl *f2* (purple), WL-RP1 (cyan), WL-RP2 (blue), FRL-RP1 (brown), and FRL-RP2 (maroon). The trapping rates are highlighted yellow. Red numbers indicate the free energy relative to Bulk Chl *a* (in units of k_BT = 25.2 meV). For clarity the free Chl *a* and Chl *f* and their decay rates have been omitted. The assumed initial population (with 400 nm excitation) is given in the Table at the bottom right.

Next, we discuss the populations of WL-PSI (dashed) and FRL-PSI (solid) of CT7203 in Figure 6G. From the WL-PSI amplitude matrix (Table S2A) we observe lifetimes of 0.66 and 1.60 ps related to direct charge separation and ultrafast equilibration between Bulk Chl *a*, Red Chl *a1* and WL-RC. The lifetime of 10.3 ps shows mainly rise of the Red Chl *a2* and WL-RP1. WL-RP1 decays to WL-RP2 in 16.5 ps. Finally, the excitations in the fully equilibrated WL-PSI are trapped in 39 ps. The quantum yield in WL-PSI is 98.7%. From the FRL-PSI amplitude matrix (Table S2B) we observe ultrafast equilibration between Bulk Chl *a*, Red Chl *a1*, Chl *f1*, and FRL-RC in 1.35 ps. Subsequently, FRL-RP1 rises with time constants of 2.44 ps (due to the 6.5% direct excitation of the FRL-RC) and 6.4 ps. The Bulk Chl *a*, Red Chl *a*, and Chl *f* antenna pigments further equilibrate in 6.4 ps, with a strong decay of Red Chl *a1*. FRL-RP1 decays to FRL-RP2 in 16.1 ps. The Red Chl *a2* pigments equilibrate with the Chl *f* antenna pigments in 22 ps. The Chl *f1* and Chl *f2* pigments equilibrate with a 56 ps time constant. Finally, the excitations in the fully equilibrated FRL-PSI are trapped in 143 ps. The quantum yield in FRL-PSI is still 96.5% (because of the small natural decay rate of 0.27 ns^{-1}). The

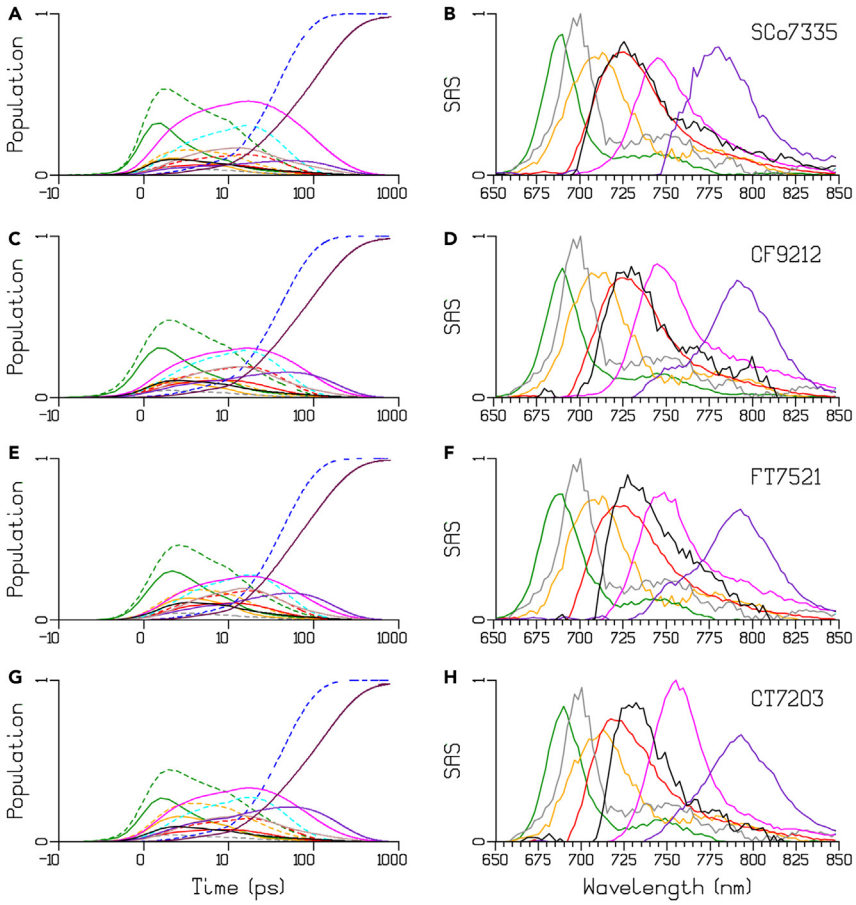

Figure 6. Estimated populations and SAS of WL-PSI and FRL-PSI of SCo7335, CF9212, FT7521, and CT7203

Populations using the kinetic schemes of Figure 5 are drawn in panels A, C, E, and G, respectively. Line type key: WL-PSI (dashed) and FRL-PSI (solid).). Color key: Bulk Chl *a* (dark green), Red Chl *a1* (orange), Red Chl *a2* (red), WL-RC (gray), FRL-RC (black), Chl *f1* (magenta), Chl *f2* (purple), WL-RP1 (cyan), WL-RP2 (blue), FRL-RP1 (brown), and FRL-RP2 (maroon). Note that the time axis is linear until 10 ps and logarithmic thereafter. SAS of the excited states of SCo7335, CF9212, FT7521, and CT7203 (B, D, F, and H). For presentation purposes, the free Chl *a*/*f* population and SAS (Figure S6) have been omitted.

populations of the Bulk and Red Chl *a* (dark green, orange, and red in Figures 6A, 6C, 6E, and 6G) in WL-PSI (dashed lines) are higher than in FRL-PSI (solid lines). In WL-PSI the excitations are trapped by the WL-RC in ≈ 39 ps, whereas in FRL-PSI most of the excitations pass through the Chl *f1* and Chl *f2* compartments (magenta and purple in Figures 6A, 6C, 6E, and 6G), before being trapped by the FRL-RC in 121–143 ps (Table 2).

The estimated SAS (Figure 6; Table 3) exhibit smooth bands with maxima at ≈689 nm (Bulk Chl *a*), ≈699 nm (WL-RC, gray), ≈726–731 nm (FRL-RC, black), ≈711 nm (Red Chl *a1*), ≈725 nm (Red Chl *a2*), ≈746–755 nm (Chl *f1*), and ≈780–797 nm (Chl *f2*). The wavelengths of the Chl *f* maxima are shortest with SCo7335, and longest with CT7203. The shapes and positions of the FRL-RC SAS resemble those of the Red Chl *a2* SAS, suggesting that an excitonic interaction within the FRL-RC is responsible for the shift to lower energy. The SAS of the WL-RC is the most difficult to estimate, it requires a guidance spectrum[52] since its population is small (gray curves in Figures 6A, 6C, 6E, and 6G). On the contrary, in a linked target analysis of the CF9212, FT7521, and CT7203 strains, the RC SAS of FRL-PSI can be estimated without any guidance. Its peak ranges from ≈726 to 731 nm, cf. Figure 6 (black SAS).

The rate constant of the primary charge separation was kept fixed at 900 ns^{-1} in the WL-PSI complexes. However, in FRL-PSI complexes the free energy of the RC* is lower than in WL-PSI by ≈ 3.2 k_BT (Figure 5), which is comparable to the difference in enthalpy of ≈2.8 k_BT (Table S5). This reduces the driving force for the primary charge separation, resulting in a decreased rate of 300 ns^{-1}. This rate can be estimated in FRL-PSI because the FRL-RC SAS can be resolved from the data (black in Figure 6). The FRL-RP1 and WL-RP1 free energies have been assumed similar, but the reduction of the free energy difference with the RC, from more than 5 k_BT in WL-RC to 2 k_BT in FRL-RC, results in an appreciable charge recombination rate of 41 ns^{-1}.

The kinetic scheme of the target analysis of FRL-PSI (Figure 5) can be interpreted thermodynamically. Thanks to the excellent connectivity of the FRL-RC and the Chl *f* compartments the excitations residing on Chl *f* can still be efficiently trapped after uphill EET, because of the still fast enough charge separation rate of 300 ns^{-1}. From the decomposition of the steady state absorption spectra, Table S5,[30] there are almost 6 Chl *f1* and ≈2 Chl *f2* pigments. Thus, the Chl *f1* has a relative entropy advantage of ln(3) = 1.1 k_BT which is counterbalanced by the enthalpy

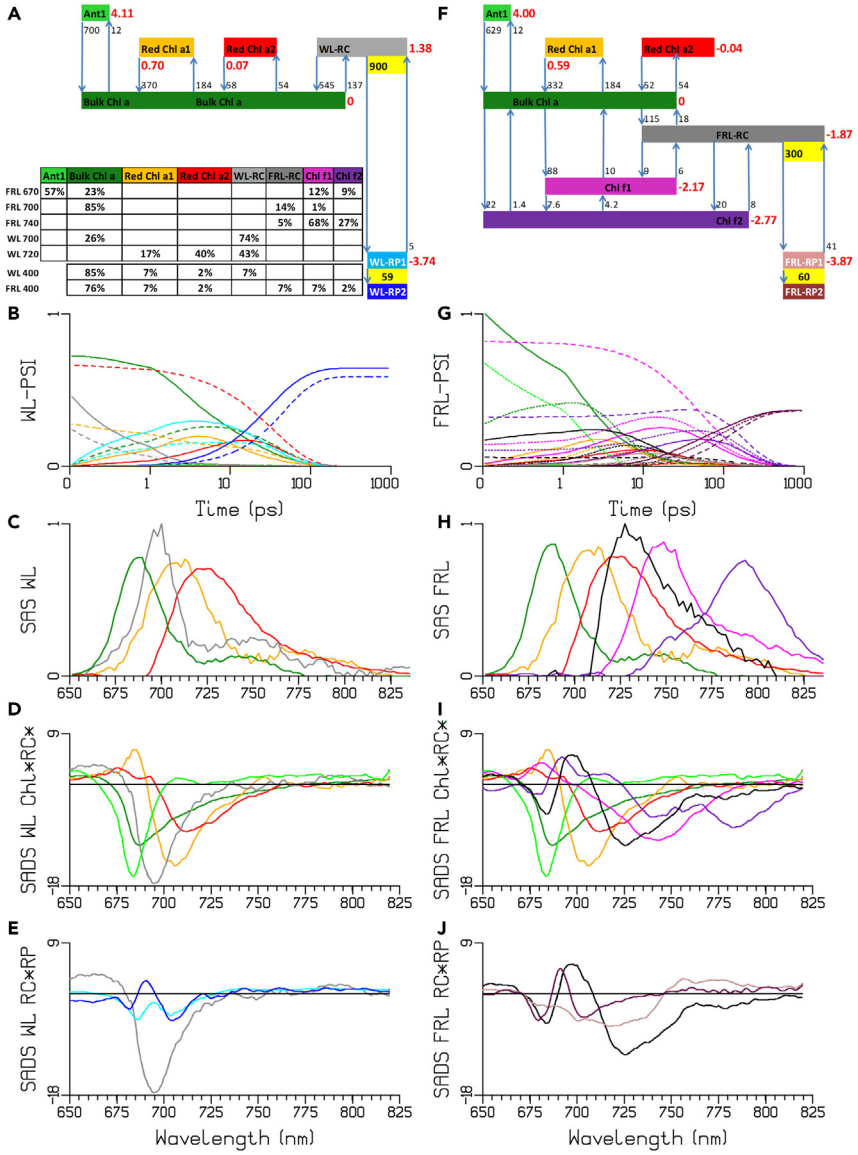

Figure 7. Target analysis of transient absorption from WL-PSI and FRL-PSI complexes of FT7521

Kinetic scheme with rates in ns^{-1} of PSI complexes of WL-PSI (A) and FRL-PSI (F) of FT7521 at 6°C. Each compartment is represented by a colored box. Key: Ant1 (light green), Bulk Chl *a* (dark green), Red Chl *a1* (orange), Red Chl *a2* (red), WL-RC (gray), FRL-RC (black), Chl *f1* (magenta), Chl *f2* (purple), WL-RP1 (cyan), WL-RP2 (blue), FRL-RP1 (brown), and FRL-RP2 (maroon). The initial populations with different excitation wavelengths are indicated in the Table in panel A, below left. The trapping rates are highlighted yellow. For clarity the natural decay rates of the excited states have been omitted. Red numbers indicate the free energy relative to Bulk Chl *a* (in units of k_BT = 24.0 meV). Estimated populations and SADS (in mOD) of WL-PSI (B, solid 700, dashed 720 nm excitation) and FRL-PSI (G, solid 700, dashed 740, dotted 670 nm excitation) of FT7521. Note that the time axis is linear until 1 ps and logarithmic thereafter. SADS of the excited states and of RP1 and RP2 (D, E, I, and J). The SAS from Figure 6F have been redrawn in (C and H) for comparison.

advantage of Chl *f2*, resulting in similar Gibbs free energies of the Chl *f1* and Chl *f2* compartments (difference less than k_BT, Table S6A). The properties of the FRL-RC differ from the WL-RC. The Gibbs free energy is lowered by ≈ 3.2 k_BT (Figures 5, 7A, and 7F; Tables S6 and S7 for transient absorption), and concomitantly the wavelength of the maximum of the emission shifts to the red by ≈ 29 nm (equivalent to ≈2.8 k_BT) (Tables S5 and S7 for transient absorption). Further discussion can be found in the supplemental information section *Thermodynamic considerations*.

In a study by Gisriel et al.,[22] it was established that there is no Chl *f* in the RC, thus the structural basis of the difference between WL-RC and FRL-RC remains to be investigated. It is suggested that an excitonic interaction within the FRL-RC is responsible for the shift to lower energy, analogous to the difference between Bulk Chl *a* and Red Chl *a2*. A possible candidate is a changed excitonic interaction involving the ec2A/ec3A dimer.[34]

Table 2. Trapping lifetimes (in ps)

	WL-PSI	FRL-PSI
SCo7335	34	128
CF9212	39	127
FT7521	41	121
CT7203	39	143

Target analysis of transient absorption in WL-PSI and FRL-PSI of FT7521

The global analysis which is detailed in the supplemental information section *Global analysis of the transient absorption dynamics of WL-PSI and FRL-PSI of FT7521* demonstrates that these data are consistent with the emission (Figure S12) and with the transient absorption dynamics of SCy6803 WL-PSI (Figure S11). It also explains why the target analysis of the transient absorption in WL-PSI and FRL-PSI of FT7521 is based upon a mixture of reduced and photo-oxidized PSI complexes. The kinetic schemes of Figures 5, 7A, and 7F, together with the initial populations with different excitation wavelengths, can describe the 5 emission and 5 transient absorption experiments in WL-PSI and FRL-PSI of FT7521. The quality of the target analysis fit is very good (Figures S9, S10, S13, and S14). After FRL excitation, the RP2 yield in reduced PSI complexes is 99% in WL-PSI (Table S8) and 96.5% in FRL-PSI (Table S9). The properties of the SADS of the excited states (Figures 7D and 7I) are generally in line with the SAS (Figures 7C and 7H) showing minima in the SADS (attributable to BL + SE) near the positions of the maxima of the SAS, cf. Tables 3 and S7. There is, however, one important exception: the Chl *f2* maximum in the SAS was at 795 nm, whereas the minimum in the SADS is around 769 nm. In the steady state absorption the Chl *f2* maximum was at 771 nm.[30] In agreement with Table 3, the secondary peak in the steady state emission was at 789 nm,[30] which indicates a large Stokes' shift of ≈18 nm. This is a consequence of the excitonic character of the Chl *f2* species, which also shows up in the broad bleach with a shoulder at ≈735 nm (purple in Figure 7I). The WL-PSI SADS of FT7521 (Figures 7D and 7E) generally agree with those of SCy6803 (Figure 4). The WL-RP1 SADS (cyan in Figure 7E) also shows a minimum around 685 nm, which agrees with the literature.[27,40,49] Interestingly, the FRL-RC SADS (black in Figures 7I and 7J) shows a large BL + SE around 728 nm, which agrees with the emission SAS (black in Figure 7H). The FRL-RP1 SADS (brown in Figure 7J) shows a broad bleach around 725 nm, indicating that the lowest excitonic state in the FRL-RC is bleached. Strikingly, the WL-RP2 and FRL-RP2 SADS are very similar, which was already pointed out by Cherepanov et al.[27] Thus, the FRL-RP2 SADS is also interpreted as a bleach of the cation (P^+700) and a large electrochromic shift around 687 nm (maroon in Figure 7J). The phylloquinone anion of FRL-RP2 does not absorb in this wavelength region. The results from an alternative target analysis without photo-oxidized PSI complexes are presented in Figure S15. The RP SADS in Figures S15D and S15H are unrealistically small, which can only be explained by the small RP quantum yield (Figures 7B and 7G), due to the mixture of reduced and photo-oxidized PSI complexes.

Conclusion and outlook

We conclude that our kinetic schemes in Figures 5, 7A, and 7F describe the entire energy transfer and trapping in both WL-PSI and FRL-PSI complexes. These schemes can further be tested and extended. A more detailed target analysis of the raw transient absorption data from WL-PSI and FRL-PSI with different excitation wavelengths could shed more light upon the ultrafast equilibration within the FRL-RC. Measurements at different temperatures[53,54] could be used to further study the thermodynamics. A target analysis of transient absorption data from mutants with different charge separation properties could further resolve the properties of the A and B branches of the PSI RC.[32,40,49] In all data we find that the properties of the FRL-RC differ from the WL-RC. The structural basis of this difference remains to be investigated.[22] The Gibbs free energy of the lowest excited state is lowered by ≈ 3.2 k_BT (Figure 5), and concomitantly the emission maximum shifts to the red by ≈ 29 nm (equivalent to ≈2.8 k_BT) (Tables 3 and S7; Figures 6 and 7). As a consequence, the rate of charge separation drops from ≈900 ns^{-1} in WL-RC to ≈300 ns^{-1} in FRL-RC. At room temperature this kinetic scheme consistently describes the delayed trapping in the FRL-PSI (≈130 ps, Table 2) by uphill energy transfer from the Chl *f* compartments with free energies of ≈k_BT below that of the FRL-RC (Figure 5). The excited Chl *f* decay via uphill energy transfer to the FRL-RC with an efficiency of 96%. Thus, thermal energy plus the energy of the low energy photon is utilized for charge separation. This fundamental insight into how photosynthetic organisms alter their light-harvesting machinery to environmental changes will hopefully inspire the utilization of FRL in genetically modified photosynthetic organisms and in artificial photosynthetic systems.

Table 3. Wavelength (nm) of the maximum of the estimated SAS

	Bulk Chl *a*	Red Chl *a1*	Red Chl *a2*	WL-RC	FRL-RC	Chl *f1*	Chl *f2*
SCo7335	688	712	726	699	726	747	780
CF9212	689	711	727	699	728	746	797
FT7521	688	710	724	699	731	748	795
CT7203	690	712	721	699	730	755	795

Limitations of the study

There are limitations of this study that should be considered when extending the PSI model for cyanobacteria to low temperatures. The kinetic schemes assume that the system can be considered homogeneous. However, at low temperatures the inhomogeneity of the protein structures will necessitate an inhomogeneous kinetic scheme with different Gibbs free energy levels for the Red Chl *a* and Chl *f* compartments. When extending the PSI model to green algae or higher plants, the properties of the lowest energy pigments in those organisms should be considered.

STAR★METHODS

Detailed methods are provided in the online version of this paper and include the following:

- KEY RESOURCES TABLE
- RESOURCE AVAILABILITY
  - Lead contact
  - Materials availability
  - Data and code availability
- METHOD DETAILS
  - Transient absorption experiments
  - Time resolved fluorescence spectra
  - Digitized transient absorption data of FT7521
  - Global and target analysis of time-resolved spectra

SUPPLEMENTAL INFORMATION

Supplemental information can be found online at https://doi.org/10.1016/j.isci.2023.107650.

ACKNOWLEDGMENTS

Roberta Croce, Martijn Tros, and Jan Dekker are thanked for critical reading of the manuscript and helpful discussions. Jochen Kruip and Matthias Rögner excellently isolated the SCy6803 PSI complexes. For the work carried out at the Max-Planck-Institute in Mülheim a.d. Ruhr. M.G.M. and A.R.H. acknowledge financial support by the EU Training and Research Networks "Harvest" and "Intro 2", and the Deutsche Forschungsgemreinschaft for grants DFG HO-924/3-1 as well as a member of Sonderforschungsbereich SFB 663. The Max-Planck-Institute für Chemische Energiekonversion (previously Max-Planck-Institute für Bioanorganische Chemie) is acknowledged for generous support of this work over many years.

AUTHOR CONTRIBUTIONS

M.G.M. and A.R.H. designed the Synechocystis PCC6803 experiments; M.G.M. conducted these experiments; I.H.M.v.S. and M.G.M. developed the kinetic schemes. I.H.M.v.S. analyzed the data. The crucial pyGlotaran software has been developed by J.W., S.W. and J.J.S. Writing – Original Draft, I.H.M.v.S.; Writing – Review & Editing, I.H.M.v.S., M.G.M., J.J.S. and A.R.H.

DECLARATION OF INTERESTS

The authors declare no competing interests.

INCLUSION AND DIVERSITY

We support inclusive, diverse, and equitable conduct of research.

Received: April 8, 2023
Revised: June 14, 2023
Accepted: August 11, 2023
Published: August 15, 2023

REFERENCES

1. Blankenship, R.E. (2021). Molecular Mechanisms of Photosynthesis, 3rd Edition (Wiley). 978-1-119-80001-9.
2. Jordan, P., Fromme, P., Witt, H.T., Klukas, O., Saenger, W., and Krauss, N. (2001). Three-dimensional structure of cyanobacterial photosystem I at 2.5 angstrom resolution. Nature *411*, 909–917.
3. Melkozernov, A.N., Barber, J., and Blankenship, R.E. (2006). Light Harvesting in Photosystem I Supercomplexes. Biochemistry *45*, 331–345. https://doi.org/10.1021/bi051932o.
4. Savikhin, S. (2006). Ultrafast Optical Spectroscopy of Photosystem I. In Photosystem I: The Light-Driven Plastocyanin:Ferredoxin Oxidoreductase, J.H. Golbeck, ed. (Springer Netherlands), pp. 155–175. https://doi.org/10.1007/978-1-4020-4256-0_12.

5. Croce, R., and van Amerongen, H. (2013). Light-harvesting in photosystem I. Photosynth. Res. *116*, 153–166. https://doi.org/10.1007/s11120-013-9838-x.
6. Govindjee, Shevela, D., and Björn, L.O. (2017). Evolution of the Z-scheme of photosynthesis: a perspective. Photosynth. Res. *133*, 5–15. https://doi.org/10.1007/s11120-016-0333-z.
7. Shubin, V.V., Murthy, S.D.S., Karapetyan, N.V., and Mohanty, P. (1991). Origin of the 77 K variable fluorescence at 758 nm in the cyanobacterium Spirulina platensis. Biochim. Biophys. Acta Bioenerg. *1060*, 28–36. https://doi.org/10.1016/S0005-2728(05)80115-X.
8. Wittmershaus, B.P., Woolf, V.M., and Vermaas, W.F. (1992). Temperature dependence and polarization of fluorescence from Photosystem I in the cyanobacterium Synechocystis sp. PCC 6803. Photosynth. Res. *31*, 75–87. https://doi.org/10.1007/BF00028785.
9. Pålsson, L.O., Flemming, C., Gobets, B., van Grondelle, R., Dekker, J.P., and Schlodder, E. (1998). Energy Transfer and Charge Separation in Photosystem I: P700 Oxidation Upon Selective Excitation of the Long-Wavelength Antenna Chlorophylls of *Synechococcus elongatus*. Biophys. J. *74*, 2611–2622. https://doi.org/10.1016/S0006-3495(98)77967-6.
10. Karapetyan, N.V., Holzwarth, A.R., and Rögner, M. (1999). The photosystem I trimer of cyanobacteria: molecular organization, excitation dynamics and physiological significance. FEBS Lett. *460*, 395–400. https://doi.org/10.1016/S0014-5793(99)01352-6.
11. Savikhin, S., Xu, W., Chitnis, P.R., and Struve, W.S. (2000). Ultrafast Primary Processes in PS I from Synechocystis sp. PCC 6803: Roles of P700 and A0. Biophys. J. *79*, 1573–1586. https://doi.org/10.1016/S0006-3495(00)76408-3.
12. Gobets, B., and van Grondelle, R. (2001). Energy transfer and trapping in photosystem I. Biochim. Biophys. Acta *1507*, 80–99.
13. Gobets, B., van Stokkum, I.H., Rögner, M., Kruip, J., Schlodder, E., Karapetyan, N.V., Dekker, J.P., and van Grondelle, R. (2001). Time-resolved fluorescence emission measurements of photosystem I particles of various cyanobacteria: A unified compartmental model. Biophys. J. *81*, 407–424.
14. Slavov, C., El-Mohsnawy, E., Rögner, M., and Holzwarth, A.R. (2009). Trapping kinetics in isolated cyanobacterial PS I complexes. Chem. Phys. *357*, 163–170. https://doi.org/10.1016/j.chemphys.2008.12.021.
15. van Stokkum, I.H.M., Desquilbet, T.E., van der Weij-de Wit, C.D., Snellenburg, J.J., van Grondelle, R., Thomas, J.-C., Dekker, J.P., and Robert, B. (2013). Energy Transfer and Trapping in Red-Chlorophyll-Free Photosystem I from Synechococcus WH 7803. J. Phys. Chem. B *117*, 11176–11183. https://doi.org/10.1021/jp401364a.
16. Toporik, H., Khmelnitskiy, A., Dobson, Z., Riddle, R., Williams, D., Lin, S., Jankowiak, R., and Mazor, Y. (2020). The structure of a red-shifted photosystem I reveals a red site in the core antenna. Nat. Commun. *11*, 5279. https://doi.org/10.1038/s41467-020-18884-w.
17. Akhtar, P., Biswas, A., Kovács, L., Nelson, N., and Lambrev, P.H. (2021). Excitation energy transfer kinetics of trimeric, monomeric and subunit-depleted Photosystem I from Synechocystis PCC 6803. Biochem. J. *478*, 1333–1346. https://doi.org/10.1042/bcj20210021.
18. Gobets, B., Valkunas, L., and van Grondelle, R. (2003). Bridging the Gap between Structural and Lattice Models: A Parameterization of Energy Transfer and Trapping in Photosystem I. Biophys. J. *85*, 3872–3882. https://doi.org/10.1016/S0006-3495(03)74802-4.
19. Gan, F., Zhang, S., Rockwell, N.C., Martin, S.S., Lagarias, J.C., and Bryant, D.A. (2014). Extensive remodeling of a cyanobacterial photosynthetic apparatus in far-red light. Science *345*, 1312–1317. https://doi.org/10.1126/science.1256963.
20. Chen, M., Schliep, M., Willows, R.D., Cai, Z.-L., Neilan, B.A., and Scheer, H. (2010). A Red-Shifted Chlorophyll. Science *329*, 1318–1319. https://doi.org/10.1126/science.1191127.
21. Li, Y., Scales, N., Blankenship, R.E., Willows, R.D., and Chen, M. (2012). Extinction coefficient for red-shifted chlorophylls: Chlorophyll d and chlorophyll f. Biochim. Biophys. Acta *1817*, 1292–1298. https://doi.org/10.1016/j.bbabio.2012.02.026.
22. Gisriel, C.J., Flesher, D.A., Shen, G., Wang, J., Ho, M.-Y., Brudvig, G.W., and Bryant, D.A. (2022). Structure of a photosystem I-ferredoxin complex from a marine cyanobacterium provides insights into far-red light photoacclimation. J. Biol. Chem. *298*, 101408. https://doi.org/10.1016/j.jbc.2021.101408.
23. Kaucikas, M., Nürnberg, D., Dorlhiac, G., Rutherford, A.W., and van Thor, J.J. (2017). Femtosecond Visible Transient Absorption Spectroscopy of Chlorophyll f-Containing Photosystem I. Biophys. J. *112*, 234–249. https://doi.org/10.1016/j.bpj.2016.12.022.
24. Nürnberg, D.J., Morton, J., Santabarbara, S., Telfer, A., Joliot, P., Antonaru, L.A., Ruban, A.V., Cardona, T., Krausz, E., Boussac, A., et al. (2018). Photochemistry beyond the red limit in chlorophyll f–containing photosystems. Science *360*, 1210–1213. https://doi.org/10.1126/science.aar8313.
25. Kurashov, V., Ho, M.-Y., Shen, G., Piedl, K., Laremore, T.N., Bryant, D.A., and Golbeck, J.H. (2019). Energy transfer from chlorophyll f to the trapping center in naturally occurring and engineered Photosystem I complexes. Photosynth. Res. *141*, 151–163. https://doi.org/10.1007/s11120-019-00616-x.
26. Zamzam, N., Kaucikas, M., Nürnberg, D.J., Rutherford, A.W., and van Thor, J.J. (2019). Femtosecond infrared spectroscopy of chlorophyll f-containing photosystem I. Phys. Chem. Chem. Phys. *21*, 1224–1234. https://doi.org/10.1039/C8CP05627G.
27. Cherepanov, D.A., Shelaev, I.V., Gostev, F.E., Aybush, A.V., Mamedov, M.D., Shen, G., Nadtochenko, V.A., Bryant, D.A., Semenov, A.Y., and Golbeck, J.H. (2020). Evidence that chlorophyll f functions solely as an antenna pigment in far-red-light photosystem I from Fischerella thermalis PCC 7521. Biochim. Biophys. Acta Bioenerg. *1861*, 148184. https://doi.org/10.1016/j.bbabio.2020.148184.
28. Tros, M., Bersanini, L., Shen, G., Ho, M.-Y., van Stokkum, I.H.M., Bryant, D.A., and Croce, R. (2020). Harvesting far-red light: Functional integration of chlorophyll f into Photosystem I complexes of Synechococcus sp. PCC 7002. Biochim. Biophys. Acta Bioenerg. *1861*, 148206. https://doi.org/10.1016/j.bbabio.2020.148206.
29. Mascoli, V., Bersanini, L., and Croce, R. (2020). Far-red absorption and light-use efficiency trade-offs in chlorophyll f photosynthesis. Nat. Plants *6*, 1044–1053. https://doi.org/10.1038/s41477-020-0718-z.
30. Tros, M., Mascoli, V., Shen, G., Ho, M.-Y., Bersanini, L., Gisriel, C.J., Bryant, D.A., and Croce, R. (2021). Breaking the Red Limit: Efficient Trapping of Long-Wavelength Excitations in Chlorophyll-f-Containing Photosystem I. Chem *7*, 155–173. https://doi.org/10.1016/j.chempr.2020.10.024.
31. Trinkunas, G., and Holzwarth, A.R. (1996). Kinetic modeling of exciton migration in photosynthetic systems. 3. Application of genetic algorithms to simulations of excitation dynamics in three-dimensional photosystem I core antenna/reaction center complexes. Biophys. J. *71*, 351–364. https://doi.org/10.1016/S0006-3495(96)79233-0.
32. Cherepanov, D.A., Shelaev, I.V., Gostev, F.E., Petrova, A., Aybush, A.V., Nadtochenko, V.A., Xu, W., Golbeck, J.H., and Semenov, A.Y. (2021). Primary charge separation within the structurally symmetric tetrameric Chl2APAPBChl2B chlorophyll exciplex in photosystem I. J. Photochem. Photobiol., B *217*, 112154. https://doi.org/10.1016/j.jphotobiol.2021.112154.
33. van Grondelle, R., Dekker, J.P., Gillbro, T., and Sundström, V. (1994). Energy-Transfer and Trapping in Photosynthesis. Biochim. Biophys. Acta *1187*, 1–65.
34. Gorka, M., Charles, P., Kalendra, V., Baldansuren, A., Lakshmi, K.V., and Golbeck, J.H. (2021). A dimeric chlorophyll electron acceptor differentiates type I from type II photosynthetic reaction centers. iScience *24*, 102719. https://doi.org/10.1016/j.isci.2021.102719.
35. van Stokkum, I.H.M., van Oort, B., van Mourik, F., Gobets, B., and van Amerongen, H. (2008). (Sub)-Picosecond Spectral Evolution of Fluorescence Studied with a Synchroscan Streak-Camera System and Target Analysis. In Biophysical Techniques in Photosynthesis Vol. II, T.J. Aartsma and J. Matysik, eds. (Springer), pp. 223–240.
36. van Grondelle, R., Dekker, J.P., Gillbro, T., and Sundstrom, V. (1994). Energy transfer and trapping in photosynthesis. Biochim. Biophys. Acta Bioenerg. *1187*, 1–65.
37. Slavov, C., Ballottari, M., Morosinotto, T., Bassi, R., and Holzwarth, A.R. (2008). Trap-Limited Charge Separation Kinetics in Higher Plant Photosystem I Complexes. Biophys. J. *94*, 3601–3612.
38. Müller, M.G., Niklas, J., Lubitz, W., and Holzwarth, A.R. (2003). Ultrafast transient absorption studies on Photosystem I reaction centers from Chlamydomonas reinhardtii. 1. A new interpretation of the energy trapping and early electron transfer steps in Photosystem I. Biophys. J. *85*, 3899–3922. https://doi.org/10.1016/s0006-3495(03)74804-8.
39. Holzwarth, A.R., Müller, M.G., Niklas, J., and Lubitz, W. (2006). Ultrafast Transient Absorption Studies on Photosystem I Reaction Centers from *Chlamydomonas reinhardtii*. 2: Mutations near the P700 Reaction Center Chlorophylls Provide New Insight into the Nature of the Primary Electron Donor. Biophys. J. *90*, 552–565. https://doi.org/10.1529/biophysj.105.059824.
40. Müller, M.G., Slavov, C., Luthra, R., Redding, K.E., and Holzwarth, A.R. (2010). Independent initiation of primary electron transfer in the two branches of the photosystem I reaction

center. Proc. Natl. Acad. Sci. USA *107*, 4123–4128. https://doi.org/10.1073/pnas.0905407107.

41. Müller, M.G., Hucke, M., Reus, M., and Holzwarth, A.R. (1996). Annihilation processes in the isolated D1-D2-cyt-b559 reaction center complex of photosystem II. An intensity-dependence study of femtosecond transient absorption. J. Phys. Chem. *100*, 9537–9544.
42. Snellenburg, J.J., Dekker, J.P., van Grondelle, R., and van Stokkum, I.H.M. (2013). Functional Compartmental Modeling of the Photosystems in the Thylakoid Membrane at 77 K. J. Phys. Chem. B *117*, 11363–11371. https://doi.org/10.1021/jp4031283.
43. van Stokkum, I.H.M., Larsen, D.S., and van Grondelle, R. (2004). Global and target analysis of time-resolved spectra. Biochim. Biophys. Acta *1657*, 82–104. https://doi.org/10.1016/j.bbabio.2004.04.011.
44. Cherepanov, D.A., Shelaev, I.V., Gostev, F.E., Mamedov, M.D., Petrova, A.A., Aybush, A.V., Shuvalov, V.A., Semenov, A.Y., and Nadtochenko, V.A. (2017). Mechanism of adiabatic primary electron transfer in photosystem I: Femtosecond spectroscopy upon excitation of reaction center in the far-red edge of the QY band. Biochim. Biophys. Acta Bioenerg. *1858*, 895–905. https://doi.org/10.1016/j.bbabio.2017.08.008.
45. Shelaev, I.V., Gostev, F.E., Mamedov, M.D., Sarkisov, O.M., Nadtochenko, V.A., Shuvalov, V.A., and Semenov, A.Y. (2010). Femtosecond primary charge separation in Synechocystis sp. PCC 6803 photosystem I. Biochim. Biophys. Acta *1797*, 1410–1420. https://doi.org/10.1016/j.bbabio.2010.02.026.
46. Schoffman, H., and Keren, N. (2019). Function of the IsiA pigment–protein complex *in vivo*. Photosynth. Res. *141*, 343–353. https://doi.org/10.1007/s11120-019-00638-5.
47. Chen, C., Gong, N., Li, Z., Sun, C., and Men, Z. (2017). Concentration Effect on Quenching of Chlorophyll a Fluorescence by All-Trans-β-Carotene in Photosynthesis. Molecules *22*, 1585.
48. Kleima, F.J., Gradinaru, C.C., Calkoen, F., van Stokkum, I.H., vanGrondelle, R., and vanAmerongen, H. (1997). Energy transfer in LHCII monomers at 77K studied by sub-picosecond transient absorption spectroscopy. Biochemistry *36*, 15262–15268.
49. Badshah, S.L., Sun, J., Mula, S., Gorka, M., Baker, P., Luthra, R., Lin, S., van der Est, A., Golbeck, J.H., and Redding, K.E. (2018). Mutations in algal and cyanobacterial Photosystem I that independently affect the yield of initial charge separation in the two electron transfer cofactor branches. Biochim. Biophys. Acta Bioenerg. *1859*, 42–55. https://doi.org/10.1016/j.bbabio.2017.10.003.
50. Guergova-Kuras, M., Boudreaux, B., Joliot, A., Joliot, P., and Redding, K. (2001). Evidence for two active branches for electron transfer in photosystem I. Proc. Natl. Acad. Sci. USA *98*, 4437–4442. https://doi.org/10.1073/pnas.081078898.
51. Akhtar, P., Caspy, I., Nowakowski, P.J., Malavath, T., Nelson, N., Tan, H.-S., and Lambrev, P.H. (2021). Two-Dimensional Electronic Spectroscopy of a Minimal Photosystem I Complex Reveals the Rate of Primary Charge Separation. J. Am. Chem. Soc. *143*, 14601–14612. https://doi.org/10.1021/jacs.1c05010.
52. van Stokkum, I.H., Wohlmuth, C., Würthner, F., and Williams, R.M. (2022). Energy transfer in supramolecular calix[4]arene—Perylene bisimide dye light harvesting building blocks: Resolving loss processes with simultaneous target analysis. J. Photochem. Photobiol., A *12*, 100154. https://doi.org/10.1016/j.jpap.2022.100154.
53. Nagle, J.F. (1991). Solving complex photocycle kinetics - theory and direct method. Biophys. J. *59*, 476–487.
54. van Stokkum, I.H.M., and Lozier, R.H. (2002). Target Analysis of the Bacteriorhodopsin Photocycle Using a Spectrotemporal Model. J. Phys. Chem. B *106*, 3477–3485. https://doi.org/10.1021/jp0127723.
55. Weißenborn, J., Snellenburg, J.J., Weigand, S., and van Stokkum, I.H.M. (2022). Pyglotaran: A Python Library for Global and Target Analysis. https://doi.org/10.5281/zenodo.4534043.
56. van Stokkum, I.H.M., Weißenborn, J., Weigand, S., and Snellenburg, J.J. (2023). Pyglotaran: a lego-like Python framework for global and target analysis of time resolved spectra. Photochem. Photobiol. Sci. https://doi.org/10.1007/s43630-023-00460-y.
57. Kruip, J., Boekema, E.J., Bald, D., Boonstra, A.F., and Rögner, M. (1993). Isolation and structural characterization of monomeric and trimeric photosystem I complexes (P700.FA/FB and P700.FX) from the cyanobacterium Synechocystis PCC 6803. J. Biol. Chem. *268*, 23353–23360. https://doi.org/10.1016/S0021-9258(19)49470-2.
58. van Stokkum, I.H.M., Kloz, M., Polli, D., Viola, D., Weißenborn, J., Peerbooms, E., Cerullo, G., and Kennis, J.T.M. (2021). Vibronic dynamics resolved by global and target analysis of ultrafast transient absorption spectra. J. Chem. Phys. *155*, 114113. https://doi.org/10.1063/5.0060672.
59. Kovalenko, S.A., Dobryakov, A.L., Ruthmann, J., and Ernsting, N.P. (1999). Femtosecond spectroscopy of condensed phases with chirped supercontinuum probing. Phys. Rev. *59*, 2369–2384. https://doi.org/10.1103/PhysRevA.59.2369.
60. Mascoli, V., Bhatti, A.F., Bersanini, L., van Amerongen, H., and Croce, R. (2022). The antenna of far-red absorbing cyanobacteria increases both absorption and quantum efficiency of Photosystem II. Nat. Commun. *13*, 3562. https://doi.org/10.1038/s41467-022-31099-5.

STAR★METHODS

KEY RESOURCES TABLE

REAGENT or RESOURCE	SOURCE	IDENTIFIER
Deposited data		
Spectroscopic data	this paper	https://doi.org/10.5281/zenodo.8193583
Software and algorithms		
pyglotaran v0.7.1	https://github.com/glotaran/	https://doi.org/10.5281/zenodo.8192542
Jupyter notebooks	this paper	https://doi.org/10.5281/zenodo.8193583
OriginPro	https://www.originlab.com	N/A

RESOURCE AVAILABILITY

Lead contact

Further information and requests for resources should be directed to and will be fulfilled by the lead contact, Ivo van Stokkum (i.h.m.van.stokkum@vu.nl).

Materials availability

This study did not generate new materials.

Data and code availability

- All Synechocystis PCC6803 spectroscopic data and the preprocessed spectroscopic data of the other strains used in this publication are published in https://doi.org/10.5281/zenodo.8193583. For the other spectroscopic *raw* data we refer to the original papers.[27,30]
- All original code has been deposited at Zenodo and is publicly available as of the date of publication. DOIs are listed in the key resources table. The results from this study can be reproduced with the structured problem-solving environment pyglotaran.[55,56] The specific version available at the time of this article's publication was v0.7.1 (https://doi.org/10.5281/zenodo.8192542). To use pyglotaran, it is recommended to install it through a Python package manager, like Anaconda's conda or Python's pip. It can also be sourced directly from its GitHub repository (https://github.com/glotaran/pyglotaran). Detailed installation instructions can be found in the repository's README file. The Jupyter notebooks used in conjunction with pyglotaran for the target analyses of Figure 4, 6, and 7 are published in https://doi.org/10.5281/zenodo.8193583. The GitHub repository https://github.com/glotaran/pub-2023-05-van_Stokkum_et_al, from which the results are published on Zenodo, is open to propose alternative models or interpretations by creating an issue and/or pull request.
- Any additional information required to reanalyze the data reported in this paper is available from the lead contact upon request.

METHOD DETAILS

Transient absorption experiments

All measurements described concern PSI complexes isolated from cyanobacteria. Ultrafast transient absorption experiments on PSI complexes from Synechocystis PCC6803 (hereafter SCy6803)[57] have been performed at RT (20°C) under annihilation free conditions[38,40,41] with excitation at 670 or 700 nm (Figure 1). A regenerative Titanium-Sapphire Laser system was employed which pumped an optical parametric amplifier (OPA) to excite the samples at various excitation wavelengths with an energy of a few hundred picojoule in a ≈125 μm diameter spot at a repetition rate of 3 kHz. The probe white light continuum was generated as a weak single filament in a thin 1-2 mm sapphire plate. The instrument response function (IRF) was described by a Gaussian-shape of ≈133 fs FWHM.

For the isolated PSI samples 10-40 μM PMS and 20-50 mM sodium ascorbate was added as described in order to keep the RCs in an open i.e. reduced state.[38] The OD of the sample was 0.73/mm at 680 nm (Figure 1). Furthermore, it was necessary to use a rotating cuvette which was periodically shifted in the horizontal plane to ensure a long time to recover in the order of 1 min. Time gated spectra from 638.5 to 761.5 nm were measured in two time ranges, from -1 to 4.8 ps in steps of 13.3 fs, and from 1 to 300 ps in steps of 0.5 ps.

Time resolved fluorescence spectra

The fluorescence properties of the PSI complexes of four species grown under white light (WL) or far-red light (FRL) conditions have been described in.[30] The four species are: Synechococcus sp. strain PCC 7335 (hereafter SCo7335), Chlorogloeopsis fritschii strain PCC 9212 (hereafter CF9212), Fischerella thermalis strain PCC 7521 (hereafter FT7521) and Chroococcidiopsis thermalis strain PCC 7203 (hereafter CT7203). Time gated spectra from 651.5 to 848.0 nm have been measured at RT (20°C) with a Hamamatsu C5680 synchroscan streak camera, combined with a Chromex 250IS spectrograph,[35] in three Time Ranges. The FWHM of the IRF was ≈4.4, ≈6.3 and ≈18 ps with Time Range 1, 2 and 4,

respectively. The global analyses of the four strains, and the preliminary target analysis of CT7203 of the time resolved fluorescence spectra after 400 nm excitation have been presented in.[30]

Digitized transient absorption data of FT7521

The transient absorption data of FT7521 measured at 6°C (with excitation wavelengths of 670, 700, 720 or 740 nm) have been described in.[27] The data used in this article have been simulated with the help of the Evolution Associated Difference Spectra (EADS, digitized with OriginPro) and their lifetimes (Figure S11C, S11D, and S12B–S12D, cf. also Figures 5 and 9 from[27]).

Global and target analysis of time-resolved spectra

The global and target analysis methodology has been described in.[35,43,58] A Gaussian-shaped instrument response function (IRF) of ≈133 fs FWHM is used, with parameters μ for the time of the IRF maximum and Δ for the FWHM of the IRF. The wavelength dependence of the parameter μ is described by a first order polynomial in the wavenumber domain.[59] A "coherent artefact" (CA) straddling time zero is present in the transient absorption of Figures 2, and S1. This is modelled with a term $IRF(\mu,\Delta).IRFAS$. It contains a matrix $IRF(\mu,\Delta)$ with the zeroth, first and second derivative of the IRF,[58,59] cf. Figure S4A. In addition, with 670 nm excitation a damped oscillation[58] (Figure S4D) is present.

Figures 5, 7A, and 7F summarize the different kinetic schemes for the WL and FRL samples. Between these samples the common SAS (Bulk Chl *a* (dark green), Red Chl *a1* (orange), Red Chl *a2* (red), WL-RC (grey)) and the rate parameters are linked as much as possible. To limit the number of free parameters in the complicated kinetic schemes (Figures 5, 7A, and 7F) a simultaneous target analysis of all 20 WL and FRL emission data sets *and* the five FT7521 transient absorption data sets has been performed with the help of pyglotaran,[55,56] and the thus estimated SAS of Bulk Chl *a*, Red Chl *a1* and *a2*, WL-RC and FRL-RC have been used to guide these SAS[52] in the simultaneous target analysis of the WL and FRL samples of an individual strain. The SAS of RP1 and RP2 are zero. During the development of the model it was assumed that several other SAS are zero in certain wavelength ranges: Red Chl *a2* (below 683 nm), Chl *f1* (below 700 nm), Chl *f2* (below 720 nm), FRL-RC (below 702 nm, or 692 nm with SCo7335), free Chl *f* (below 700 nm, cf. Figure S6A). However, in the final target analysis presented in Figure 6 the only restriction needed was on the long lived free Chl *f*. An area penalty for the Species Associated Spectra (SAS) is employed to estimate the equilibria.[42] It was assumed that the Chl *f* SAS area is 35% larger than the Bulk Chl *a* SAS area, since the Chl *f* spectrum is broader (cf. Figure 1 from[21] and[60]). Care was taken that the detailed balance conditions were obeyed.[53] Detailed balance implies that the products of the rate constants clockwise and counterclockwise in a cycle, e.g. Bulk Chl *a* ↔ Chl *f1* ↔ FRL-RC ↔ Bulk Chl *a*, must be equal. This is equivalent to a zero sum of the Gibbs free energy in a cycle. The transient absorption data of FT7521 data have been measured at 6°C, thus additional assumptions on the constancy of the SADS and downhill rate constants between 6°C and RT were needed. Thus, the differences between the kinetic schemes of FT7521 at RT (Figure 5C) and at 6°C (Figures 7A and 7F) are limited to small differences in the ΔG and in the uphill rate constants, and no additional free parameters have been introduced.

The estimated SAS and SADS are subsequently fitted using a skewed Gaussian shape[43] (Figure S6). The enormous complexity of this target analysis can only be mastered with the help of the structured problem solving environment pyglotaran,[55,56] which enables simultaneous target analysis of different groups of data (emission and transient absorption, 25 data sets in total) using different types of minimization (nonnegative least squares for the nonnegative SAS vs. ordinary least squares for the SADS) estimating more than 100 nonlinear parameters with the help of nonlinear least squares. These more than 100 nonlinear parameters consist of rate constants in the kinetic schemes (Figures 5, 7A and 7F), the parameters that describe the IRF of all experiments, the relative scaling parameters of the data sets that are being fitted simultaneously, the inputs to the compartments (cf. the Table at the bottom left of Figure 7A), and the parameters that describe the small amounts of free Chl *a* and of free Chl *f* in each experiment. The relative precision of the estimated parameters is 10%.